



Preliminary evaluation of laser-induced breakdown spectroscopy for tissue classification[☆]

Fang-Yu Yueh^a, Hongbo Zheng^b, Jagdish P. Singh^{a,*}, Shane Burgess^c

^a Institute for Clean Energy Technology, Mississippi State University, Starkville, MS 39759, United States

^b Department of Applied Physics, Nanjing University of Technology, Nanjing, Jiangsu, 210009, China

^c College of Veterinary Medicine, Mississippi State University, Mississippi State, MS 39762, United States

ARTICLE INFO

Article history:

Received 1 December 2008

Accepted 23 July 2009

Available online 5 August 2009

Keywords:

LIBS

Tissue characterization

ANN

PLS

HCA

ABSTRACT

Laser-induced breakdown spectroscopy (LIBS) is an on-line, real-time technology that can produce immediate information about the elemental contents of tissue samples. We have previously shown that LIBS may be used to distinguish cancerous from non-cancerous tissue. In this work, we study LIBS spectra produced from chicken brain, lung, spleen, liver, kidney and skeletal muscle. Different data processing techniques were used to study if the information contained in these LIBS spectra is able to differentiate between different types of tissue samples and then identify unknown tissues. We have demonstrated a clear distinguishing between each of the known tissue types with only 21 selected analyte lines from each observed LIBS spectrum. We found that in order to produce an analytical model to work well with new sample we need to have representative training data to cover a wide range of spectral variation due to experimental or environmental changes.

© 2009 Elsevier B.V. All rights reserved.

1. Introduction

The interaction of high-power laser light with a target sample has been an active topic of research in many fields of research and analysis. When a high-power laser pulse is focused onto the target of any kind of material (solid, liquid, gas), a small amount of material is evaporated, initiating an avalanche ionization of the sample elements and creating a microplasma. The use of lasers to produce microplasmas to vaporize, dissociate, excite or ionize species on material surfaces has the potential of becoming a powerful analytical tool [1–3]. Since nano- to micro-grams of material are ablated in femto- to nano-seconds (depending on the laser pulse duration), the whole process can be considered as minimally destructive. This technique which is based on the spectroscopic study of optical emission from laser-produced plasmas to obtain information about the composition of the target material is known as laser-induced breakdown spectroscopy (LIBS). Since first observed in 1962, LIBS has been applied mostly to materials analysis, environmental monitoring and process control [1–5]. Recently, the potential of applying LIBS to biological samples has been investigated [6–12]. LIBS has been used to study biological samples, such as tissues [6,7],

gall stones [8], and biological aerosols [9]. It has been used to characterize and identify different bacteria [10,11] and to detect and identify biological agents [12].

Cancers may occur *in situ* as a result of metastasis from distant and ontologically-unrelated tissue. Rapid automated methods of differentiating malignant from non-malignant tissues could save medical pathologists time and potentially improve cancer diagnosis. We have previously described the potential for LIBS to differentiate malignant from neighboring non-malignant tissues [13,14]. Not only can LIBS be used to differentiate healthy from cancerous tissue, but it could be used to identify (or at least narrow down the identity of) the primary organ-source of a metastatic cancer. For this to be possible, however, we need to establish how well LIBS can differentiate normal tissues. Also, because LIBS measures elemental composition, it may also be useful in forensics for rapid detection of tissue origin. Here we determine whether or not normal tissues from different organs produce sufficiently different LIBS spectra to be able to identify the organ of origin. Different data processing techniques for LIBS were also evaluated for tissue identification.

2. Experimental details

2.1. Tissue samples and cooling system

Tissue blocks approximately 5–10 mm³ were taken post mortem from the brain, lung, spleen, liver, kidney and skeletal muscle of 20 normal 6-week old chickens. These tissues were divided into two groups (see Table 1). The first group, our “known samples,” had 41

[☆] This paper was presented at the 5th International Conference on Laser-Induced Breakdown Spectroscopy (LIBS 2008), held in Berlin, Adlershof, Germany, 22–26 September 2008, and is published in the Special Issue of Spectrochimica Acta Part B, dedicated to that conference.

* Corresponding author.

E-mail address: singh@icet.msstate.edu (J.P. Singh).

Table 1
Tissue samples used in this work.

| | Muscle | Kidney | Liver | Lung | Spleen | Brain |
|---------------------------------------|--------|--------|-------|------|--------|-------|
| Number of known samples | 10 | 5 | 5 | 5 | 6 | 10 |
| Number of external validation samples | 10 | 5 | 5 | 5 | 10 | 9 |

tissues. We assigned random numbers to the remaining 44 samples and these were analyzed as external validation samples (i.e. blind sample). These external validation samples were used to evaluate the classification model obtained from the known tissue samples. Tissue blocks were frozen at $-20\text{ }^{\circ}\text{C}$ prior to analysis.

Immediately prior to LIBS analysis, the tissues were transferred to a cooling unit to maintain the tissue at $-20\text{ }^{\circ}\text{C}$ during LIBS measurement. The small cooling unit, built from a Neslab circulation bath (RTE-111), was mounted on an X–Y translator. The cooling system, translator, and tissue were enclosed inside a Perspex box. A 2.5-cm hole was drilled in the top of the box to allow laser beam entry and to collect the LIBS signal. The same hole was also used to remove the ablated sample material from the box.

2.2. LIBS system

The schematic diagram of the experimental setup for tissue samples is shown in Fig. 1. The experimental details of the LIBS system is described in references [13,14]. Briefly, a frequency-doubled, Q-switched Nd:YAG laser (Continuum Surelite III) is focused onto the sample surface using an ultraviolet (UV)-grade quartz lens of 300-mm focal length. Atomic emission from the laser-induced plasma was collected by an optical fiber. The distal end of the fiber was attached to an UV–VIS echelle, broadband spectrograph (ESA3000, LLA Instruments GmbH, Berlin, Germany). The echelle spectrometer detection system is equipped with a 1024×1024 element intensified charge coupled device (ICCD) detector (Kodak KAF-1001) with a pixel width of 0.024 mm. The simultaneous spectral coverage of this detection system is from 200 to 780 nm. The linear dispersion for the echelle spectrometer system varies from 5 pm/pixel at 200 nm to 19 pm/pixel at 780 nm. The detector was operated in gated mode using a fast pulse generator DG-535 (Stanford Research Systems Inc.) and was synchronized to the laser output pulse. Data acquisition and analysis were performed using a personal computer with ESAWIN software (LLA Instruments GmbH, Berlin, Germany).

LIBS spectra were recorded under various experimental conditions to optimize the LIBS signal. Operating parameters such as laser pulse energy, detector gate time delay and width were experimentally

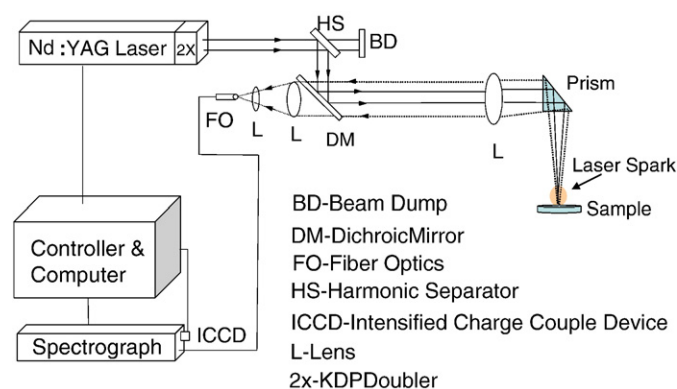


Fig. 1. Schematic diagram of LIBS experimental setup.

validated. We found that a gate delay time of $1\text{ }\mu\text{s}$, a gate width of $5\text{ }\mu\text{s}$, and a laser energy of 5 mJ/pulse provided optimal signal-to-noise ratio (S/N) for tissue measurement and therefore were used to record the LIBS spectra of all the tissue samples. Since the tissue sample surface is rough and possibly heterogeneous, we have collected 20 individual spectral frames where each frame was the sum of 10 laser shots. Finally, these 20 individual frames were averaged to obtain one resultant spectrum (i.e., each recorded spectrum is a 200-shot averaged spectrum).

3. Data analysis

Different techniques have been used to identify materials from LIBS data. The correlation technique and neural networks have been used to identify polymers [15,16]. Bohling et al. developed a fiber-optics LIBS sensor for identifying mines and explosives by analyzing the surface materials with neural networks [17]. Recently, LIBS data of three chromium-doped soils were analyzed by two chemometric techniques (i.e., principal components analysis and neural networks analysis) [18]. Multivariate techniques, such as principal components analysis (PCA), have been used to classify biological aerosols [9]. A discriminant function analysis has been used to discriminate between the biotypes and *E. coli* strains [19]. PCA and cluster analysis have been used for characterizing screen-printed electrodes with in-depth resolution [20] and for differentiating bacterial spores, molds, pollens, and protein [21]. Multivariate techniques have been used to identify preservative types and to predict elemental content in preservative-treated wood [22]. Three chemometric methods, PCA, soft independent modeling of class analogy (SIMCA) and partial least-squares discriminant analysis (PLS-DA), have been used to investigate rock identification on the surface of Mars by remote laser-induced breakdown spectroscopy [23]. In this work, we have evaluated three different techniques (i.e. cluster analysis, partial least square discriminant analysis and neural network analysis) for tissue identification. The details of those techniques can be found elsewhere and we give only brief a description of each technique.

3.1. Cluster analysis

Clustering uses statistical techniques to organize different objects with similar structure into groups and is used in many social science and biological science studies [24–27]. Here we used hierarchical cluster analysis (HCA) to identify the tissue samples. We have followed Goodacre's method [28,29] to first perform PCA to reduce the original multivariate data to a smaller number of factors while preserving most of the variance. Then discriminant function analysis (DFA) was performed. DFA uses the derived principal components and the data of repeated measurements to minimize the variation within the same group and maximize the variation between different groups. Finally, HCA uses the similarity matrix constructed from the DFA space to produce a tree diagram (also called dendrogram) using average linkage clustering. In average linkage clustering, the measure of similar structure is based on the mean distance between any member of one cluster to any member of another cluster. The PCA and DFA were performed using both Matlab 5.3 and GRAMS/AI 7.02. The Cluster Analysis Program developed by Barton [30] was used to produce dendrograms.

3.2. Partial least square discriminant analysis (PLS-DA)

Partial least square is a quantitative spectral decomposition technique that is closely related to principal component regression (PCR) [31–33]. PCR first decomposes the X-variable (e.g., sample spectral data) into a set of eigenvectors and scores, and regresses these against the Y-variable (e.g., sample properties) as a separate step.

PLS performs single step decomposition in both the *X*-variables and *Y*-variables. It uses the correlation relationship between the *X*- and *Y*-variables to decompose the variables into their most common variations. PLS generates two sets of vectors and two sets of corresponding scores: one for the *X*-, and the other for the *Y*-variables. The two sets of scores are related to each other through regression, and a calibration model is then constructed. Our optimized models were obtained by the “leave one out” cross-validation technique based on the minimum predicted residual sum of squares (PRESS). The predictive quality of the models was evaluated by calculating the standard error of cross validation (SECV) and the standard error of prediction (SEP) in the validation step with independent samples. There are two types of PLS, namely, PLS-1 and PLS-2. They are similar, but PLS-1 processes each *Y*-variable separately while PLS-2 processes all the *Y*-variables simultaneously. PLS can be used for predicting the constituents of a complex mixture. However, to achieve accurate prediction, PLS generally needs a large number of samples to build a calibration model. In this work, PLS-DA, a PLS-based classification method was used. The *Y* variables are the class assignment (i.e. tissue type) and the *X* variables are the spectral line intensity ratio. Discriminant analysis (DA) is performed in order to produce maximum separation among classes. PLS-DA was performed with GRAMS/AI 7.02 PLSplus/IQ (Thermo Galactic, Salem NH).

3.3. Neural network analysis (NNA)

Neural networks (NN) can provide solutions to classification and prediction problems with a high degree of precision and accuracy. NN has to “learn” from experience before correctly processing information [34–36]. The network consists of a large number of simple processing elements (PEs) which are densely interconnected (analogous to neurons of a human brain). With the given inputs and the related outputs, the networks learn how the inputs of each data set are associated with the output. The network continuously refines and organizes itself to fit the data, so that it produces a relatively accurate response for a given input. NN analysis uses a mathematical function to discover the relationship between the input variables and output variables. After the network learns from the training data, it uses the inferred relationship between the inputs and the corresponding outputs to make predictions for unknown input data. Training will be most effective if the training data spread throughout the input space. The performance of a NN model can be evaluated using a root mean square error of prediction (RMSEP) and a correlation coefficient (*R*). We used NeuralWare Predict (NeuralWare, Inc., Pittsburgh, PA) to test tissue identification.

4. Results

4.1. Tissue Spectra

Typical 200-shot LIBS spectra from the six different tissues are shown in Fig. 2. The major elements in the tissue samples were identified from the observed tissue spectra. The most dominant emission lines associated with those elements and suitable for LIBS analysis are given in Table 2.

4.2. Tissue identification

Each LIBS tissue spectrum (200–780 nm) contained 53,151 data points. However not every data point is useful for tissue study. Some spectral features are not significant for identification. Including these features in analysis, might cause over-fitting (i.e., fit training set perfectly but, has large error for new data). Those features should be considered as unwanted noise to the spectral analysis. Ten LIBS spectra (200 shots per spectrum) of each sample (total of 41 tissue

samples) were used in the analyses. To reduce the amount of data to be processed, we have selected only 21 analyte lines (see Table 2) as the “spectral fingerprint” for the tissue samples. Some atomic lines which were identified and listed in Table 2 were not included in this work due to their low signal-to-noise ratio. To eliminate the effect of laser shot-to-shot variation on the analysis, the area of these analyte lines were normalized by the area of the Ca 422.6-nm line. The reason for selection of the Ca 422.6-nm line as reference line is that this line was found in all tissue samples with relatively high intensity.

4.2.1. HCA

In this analysis, First, PCA is used to remove data collinearities and reduce the number of inputs to the DFA. Then DFA used the principal components (PCs) scores obtained from PCA and the knowledge of the replicates to remove any sample presentation differences. A clustering program based on the average DF scores was used to produce a dendrogram. The area ratio data of 20 analyte lines from all 41 tissue samples were used. The spectra obtained from the same tissue sample were grouped as the same class in DFA. The dendrograms were generated with different PCs (from 3 to 13). We found that 11 PCs gave the best classification results. The dendrogram for all 41 tissue samples using 11 PCs is shown in Fig. 3. Except for kidney sample Kd2 (circled in Fig. 3), all other samples are grouped correctly with the same type of tissue sample. Since only a limited number of analyte lines are used here, it is possible that the selected lines did not provide sufficient spectral features to well differentiate kidney and brain. More spectral comparisons are needed to find other spectral features (i.e., the spectral regions which are not included in this analysis) to be included in analysis to achieve better identification for these two tissues.

4.2.2. PLS

Sixty data points from each analyte line were concatenated as one data record for PLS analysis. We assigned 6 constituent values for each sample. Each sample had only one constituent value as 1 and the rest of the constituent values were zero: brain was (1,0,0,0,0,0); kidney: (0,1,0,0,0); liver: (0,0,1,0,0,0); lung: (0,0,0,1,0,0); muscle: (0,0,0,0,1,0); and spleen: (0,0,0,0,0,1). We first tested these data with a preprocessing approach of multiplicative scatter correction (MSC). We did not find any improvement with MSC as the analyte line was already normalized to the intensity of the Ca reference line. We also compared the results from both PLS-1 and PLS-2 and found PLS-2 gave slightly better results as compared with the results from PLS-1. The final analysis was done for 41 samples using PLS-2 with cross validation and 10 factors for all six constituents. A variety of statistical tests (i.e., scores are within the range of scores of the training data set data for the model; *F*-test to check that the spectral residual is statistically similar to the training set data for the model; the calculated Mahalanobis distance for the sample is less than the accepted value; and that the predicted concentration values are within the range of concentration for each constituent in the original training set) were performed to determine whether the prediction was successful. The results of the PLS-2 analysis are shown in Fig. 4. The tissue is identified as the component that is closest to 1. From Fig. 4, it is clear that the tissue from lung, muscle, spleen, and brain can be identified with confidence. However, kidney and liver were identified with a possibility of error due to more than one constituent values being much greater than 0 and also due to large standard deviations.

4.2.3. NN analysis

In NNA, the program separates all 410 data records which come from 41 samples (each sample has 10 spectra) into training and test sets to assure robust generalization. Each record consists of 21 analyte line areas obtained from one spectrum. The data were

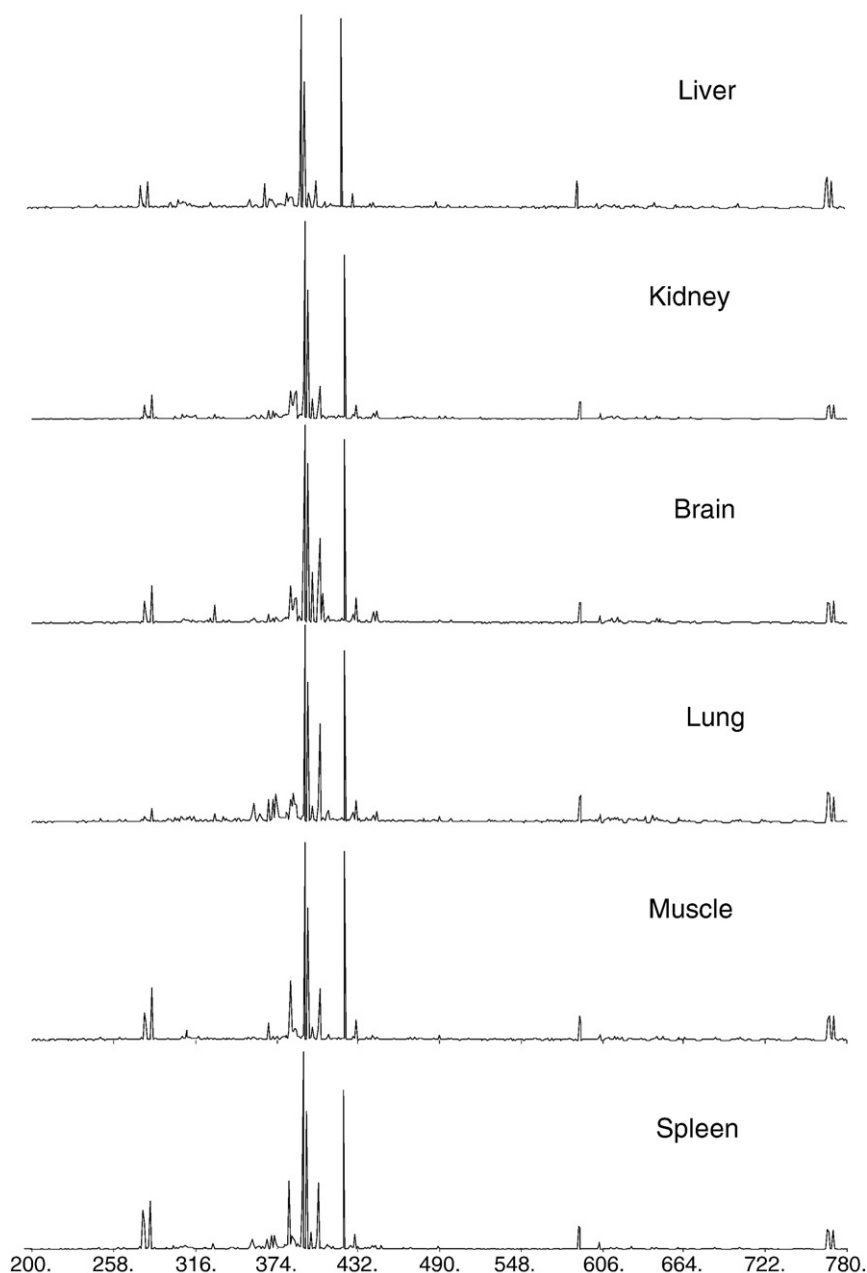


Fig. 2. LIBS tissue spectra.

Table 2

Analyte lines identified from tissue samples.

| Element | Analyte lines (nm) |
|---------|--|
| Ca | 422.673 ^a , 396.847 ^a , 431.865 ^a |
| Al | 309.270 ^a , 396.152 ^a |
| Fe | 371.993 ^a , 404.581 ^a |
| Cu | 324.754 ^a , 327.390 ^a |
| Na | 330.237 ^a , 588.995, 589.592 |
| Zn | 330.294 ^a , 307.206 ^a , 307.590 ^a |
| Cr | 357.869 ^a |
| Mg | 279.553 ^a , 285.213 ^a |
| K | 404.414 ^a , 404.721 ^a , 766.491, 769.898 |
| P | 255.328 ^a , 253.565 ^a |
| C | 247.857 ^a |
| Li | 670.796 |
| Ni | 341.476, 352.454 |
| Mo | 317.035 |
| Sn | 603.770 |
| Sc | 498.345 |

^a Analyte lines used in the HCA analysis.

processed for better distributions of values for modeling, using an algorithm based on a non-linear Kalman filtering learning rule to build the model. We have assigned arbitrary numerical values to each sample (i.e., 1 for spleen; 2 for liver; 3 for lung; 4 for muscle; 5 for kidney; 6 for brain). The predicted value was considered a correct identification when the difference between the actual value and predicted value was less than 0.5. In order to evaluate the performance of the NN model for predicting the data that it has not seen before, the NN model needed to be tested. The model's performance was tested and the results are presented in Fig. 5. Only 408 records were used in the final test because two records were considered as outliers in the initial test and were excluded. The relatively small difference between correlation values (~0.98) suggests that the model generalizes well and that it is likely to make accurate predictions when it processes unknown data. The prediction results using this model are shown in Fig. 5. The error bars in the plot represent the standard deviation obtained from 10 spectra of the same sample.

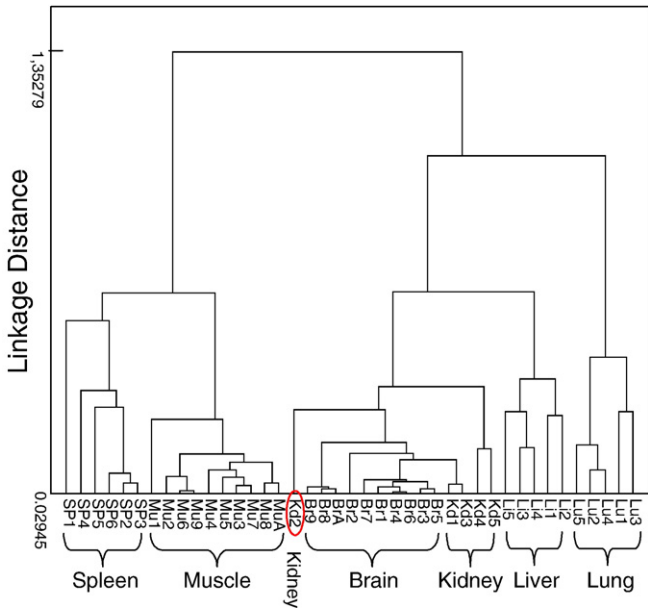


Fig. 3. The dendrogram for all 41 tissue samples.

4.3. External validation

To test if LIBS spectra alone can be used to identify the unknown tissues, we have used the techniques described above with external

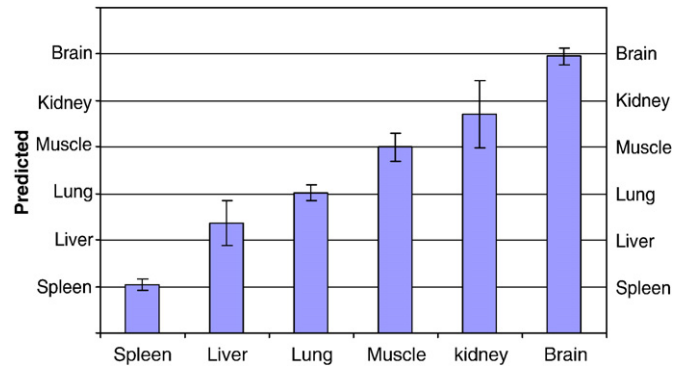


Fig. 5. Tissue analysis results using NNA.

validation sample data. The data of the external validation samples were taken on different dates from the known sample data that was used to create the model. It is a test to check if a slight difference in experimental setup, environment or system performance could cause spectral differences and consequently identification errors with a calibration model built earlier. We first used PCA to reduce the size of the data set prior to applying alternate methods of data analysis. PCA was also used to find the correlation between the spectral data in the known and external validation samples. Fig. 6 shows a plot of PCA scope for PCs 1 and 2 of the brain tissue data. The known brain tissue samples are grouped together as are the external validation brain tissue samples. However these two groups are wildly separated in

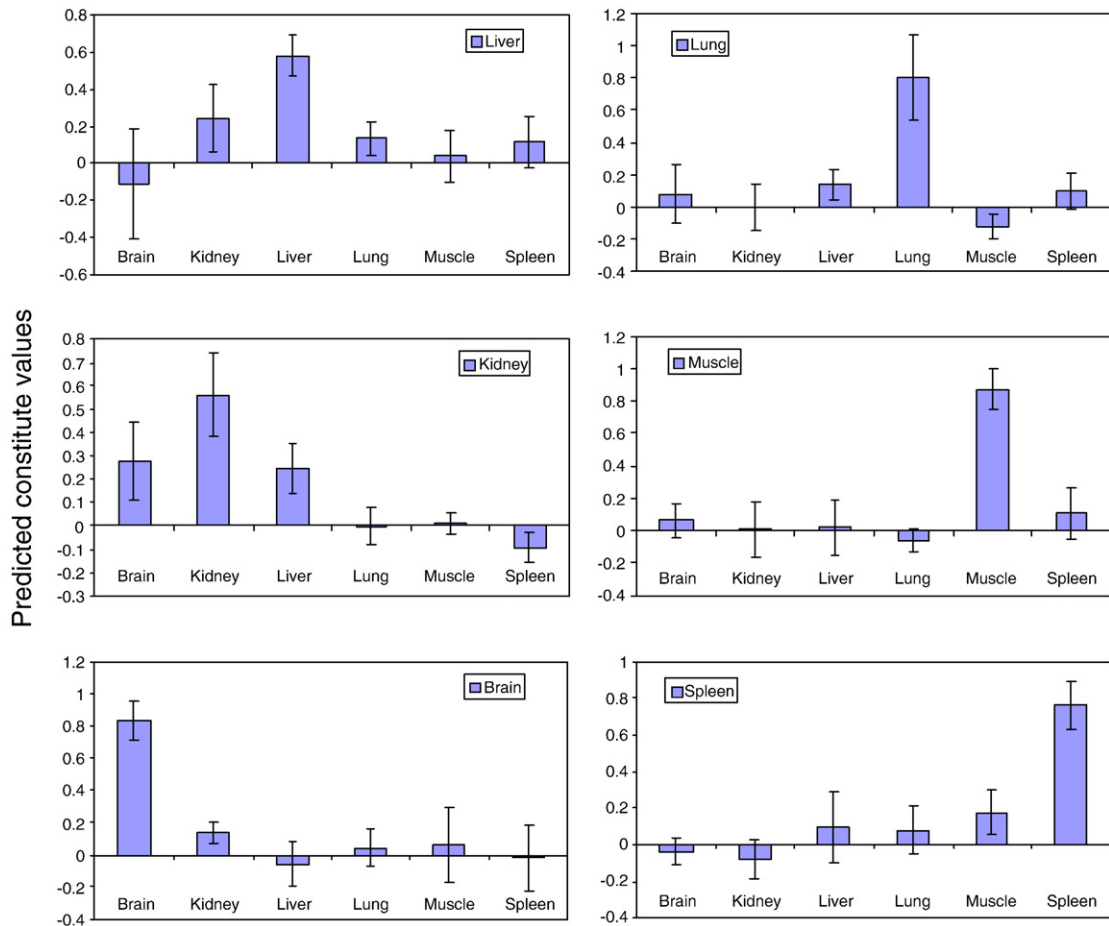


Fig. 4. Tissue analysis results using PLS-2.

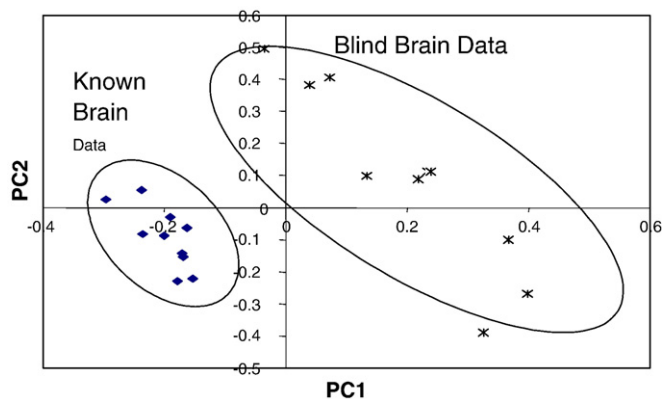


Fig. 6. Factor plot for brain tissue data and external validation brain tissue data.

PC1. This shows that it might be challenging to correctly identify external validation tissue samples with a model built previously. We can use the external validation test sample data to determine the model's long term stability.

4.3.1. HCA

The tree diagram for all external validation samples is shown in Fig. 7. It clearly shows that all the samples are grouped correctly with the same type of tissue sample except for tissue samples No. 94 (muscle), 74 (kidney), and 50 (lung). Then we performed an analysis for both known tissue samples and external validation samples. We put all data of external validation set of samples into a data array and performed HCA. Fig. 8a shows that all the external validation liver samples closely group with the known liver samples. Fig. 8b shows that except for tissue No. 50 (lung), all external validation lung sample have a short linking distance with known lung. Fig. 8c shows that all the external validation muscle tissues are more closely linked to the known muscle samples than to any other

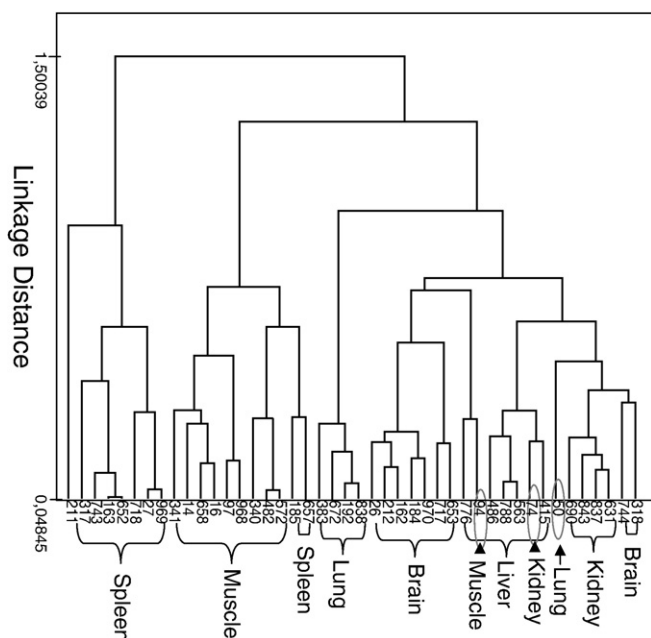


Fig. 7. The dendrogram for all external validation set of tissue samples.

known tissues. Fig. 8d shows that two external validation spleen samples grouped correctly with spleen, but the rest of them did not (although they grouped close together). Fig. 8e (brain) shows a similar case as for the external validation spleen samples. Only tissue No. 318 grouped correctly with known brain samples. Tissue No. 744 was closer to the brain–kidney group. The rest of the external validation brain samples grouped together. Fig. 8f shows that only two external validation kidney samples closely grouped with known kidney samples: one grouped with brain, and the other two were closer to the brain–kidney group than the rest of the tissues.

4.3.2. PLS

The calibration model of PLS-2 built with 41 known tissue samples was used to predict the external validation tissue sample. All 44 external validation tissue samples were analyzed with this PLS-2 calibration model. The results of PLS analysis are shown in Table 3 in which each external validation sample was assigned as correct identification (i.e., prediction match with the true tissue), incorrect identification (i.e., prediction match with others than the true tissue), or failure. The failure was determined based on the statistics tests described in Section 4.2.1. The data of external validation muscle, kidney and liver samples have 60% correct identification rates using the model built with known tissue data. However, over half of the external validation brain and spleen data failed the PLS-2 prediction test. Only about 30–45% of these data gave correct identification.

4.3.3. NN results

The NN model, which was trained and tested with all data of known tissue samples, was tested with the data of the external validation set of samples. The data of the external validation set of tissue samples, organized the same way as the training data, were input and processed by NNA. The prediction results of the external validation samples are shown in Table 4. The model performed well for muscle and spleen but not well for the other tissues. Two possible reasons that the model did not perform well are: (1.) the data used to train the model may not be statistically representative of the data population and (2.) the model may be over-fitting the data. The PCA analysis has shown a small difference in the spectral features in the unknown set that is not in the representative data (used to model). This can cause poor prediction results with NNA. It is possible to improve the NNA prediction by building neural network models that represent a wider range of experimental conditions, such as different collection dates, incident pulse energies, sample-to-lens distances, etc. Also constructing the NN model by increasing the number of data recorded with less averaging may also improve the tissue predictions.

5. Conclusions

In this work we have studied the analysis of LIBS data with chemometric techniques to identify different biological tissues. Six tissues (i.e., brain, lung, spleen, liver, kidney and skeletal muscle) from 20 normal 6-week old chickens were used in this study. We used 21 selected analyte lines from each observed LIBS spectrum in all analyses. We found that the results are reasonably good for all the known tissue samples, i.e., we could clearly distinguish (or group) between each of the tissue types. We then tested LIBS analysis on one batch of 44 tissues that were each assigned a random number. These samples were analyzed “blind”. Since data of these external validation samples were taken on different dates from the data used to train the model, slight spectral variations between the training data and test data were not properly modeled. This resulted in poorer identification results with external validation samples. This shows that in order for a model to work well, we need to have

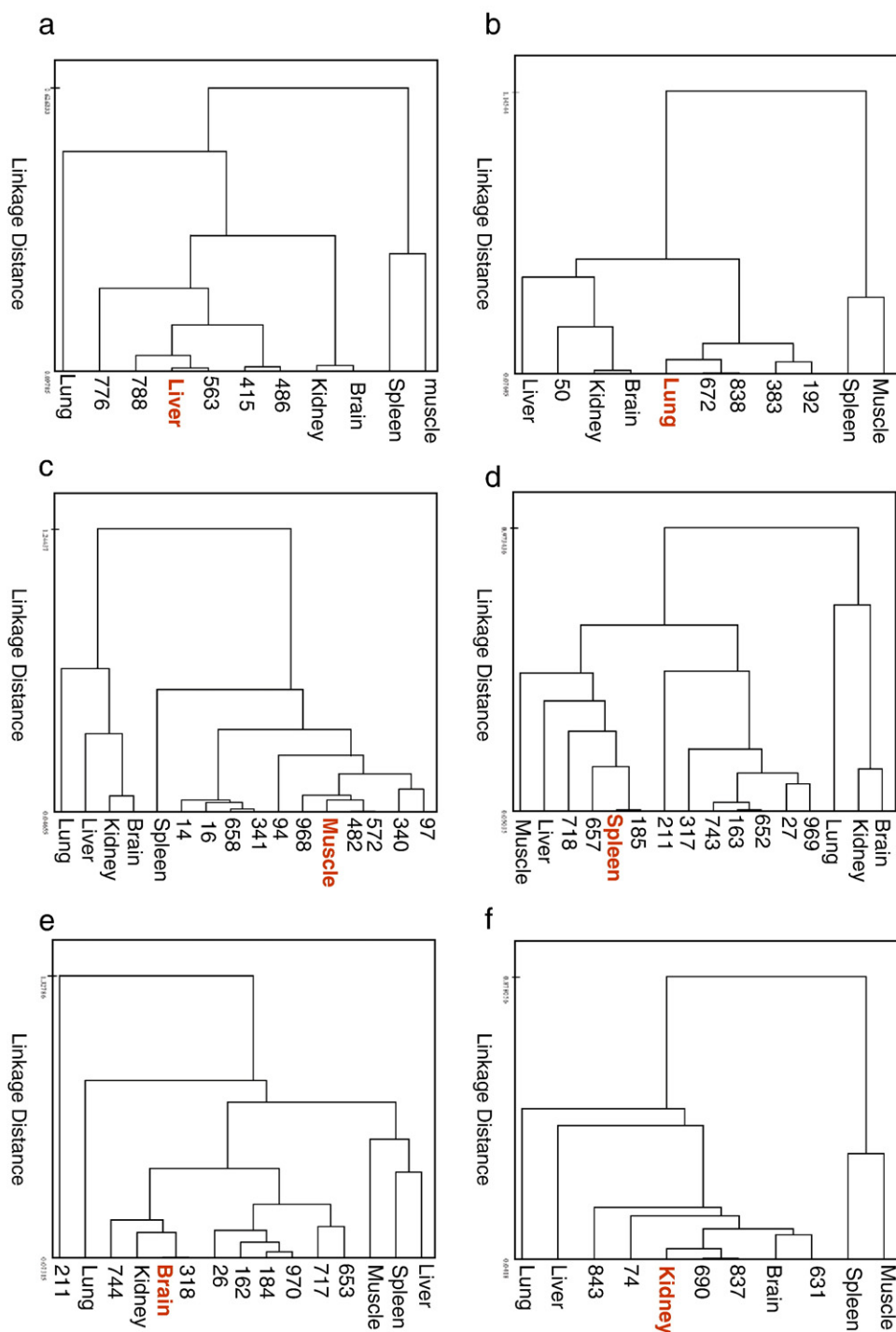


Fig. 8. The dendrogram for external validation tissue samples along with known tissue samples. a. Liver; b. Lung; c. Muscle; d. Spleen; e. Brain; f. Kidney.

representative training data to cover a wide range of spectral variation due to experimental or environmental changes. To improve the correct identification rate, the number of spectra from each sample needs to increase to improve the statistics; we need to select more spectral lines for analysis, and reject outliers. Also the selection of analyte lines plays a key role for correct identification. The selection of irrelevant lines will not help in classification and sometimes causes overfitting. The multivariate techniques are known to be efficient methods for sorting and classifying data. However, the results of this study shows that better reproducibility data are needed to produce robust classification models. More work on tissue

identification using LIBS spectroscopy will continue. The study will extend to characterize different normal animal tissues and more importantly, to differentiate tumor tissues from normal ones, and thus demonstrating medical diagnosis potential.

Acknowledgments

Financial support was provided by Mississippi State University's Life Science and Biotechnology Institute (LSBI) and by the US Department of Energy (DOE) Cooperative Agreement no. DE-FC01-

Table 3
PLS-2 results of the external validation tissue samples.

| Tissue sample | Muscle | | Lung | | Liver | | Kidney | | Spleen | | Brain | |
|-------------------------------|------------------|--------------------|------------------|--------------------|------------------|--------------------|------------------|--------------------|------------------|--------------------|------------------|--------------------|
| | No. ^a | Pred. ^b |
| External validation samples | 482 | Muscle | 672 | Lung | 776 | Fail | 843 | Brain | 163 | Fail | 717 | Fail |
| | 658 | Fail | 383 | Lung | 415 | Brain | 690 | Kidney | 185 | Fail | 744 | Brain |
| | 14 | Fail | 838 | Lung | 486 | Liver | 74 | Kidney | 27 | Fail | 162 | Brain |
| | 16 | Muscle | 192 | Lung | 788 | Liver | 631 | Brain | 317 | Fail | 184 | Fail |
| | 340 | Muscle | 50 | Lung | 563 | Liver | 837 | Kidney | 211 | Fail | 212 | Brain |
| | 341 | Fail | | | | | | | 657 | Spleen | 970 | Fail |
| | 572 | Liver | | | | | | | 718 | Liver | 653 | Fail |
| | 94 | Muscle | | | | | | | 743 | Fail | 26 | Fail |
| | 97 | Muscle | | | | | | | 969 | Spleen | 318 | Brain |
| | 968 | Muscle | | | | | | | 652 | Spleen | | |
| Correct identification rate | 6/10 | | 5/5 | | 3/5 | | 3/5 | | 3/10 | | 4/9 | |
| Fail statistics test rate | 3/10 | | 0/5 | | 1/5 | | 0/5 | | 6/10 | | 5/9 | |
| Incorrect identification rate | 1/10 | | 0/5 | | 1/5 | | 2/5 | | 1/10 | | 1/9 | |

^a Tissue number.

^b PLS-2 prediction.

Table 4
NNA results of the external validation tissue samples.

| Tissue sample | Muscle | | Brain | | Kidney | | Liver | | Lung | | Spleen | |
|-------------------------------|------------------|--------------------|------------------|--------------------|------------------|--------------------|------------------|--------------------|------------------|--------------------|------------------|--------------------|
| | No. ^a | Pred. ^b |
| External validation samples | 482 | Muscle | 717 | Muscle | 843 | Kidney | 776 | Muscle | 672 | Lung | 185 | Spleen |
| | 658 | Muscle | 744 | Brain | 690 | Muscle | 415 | Lung | 383 | Muscle | 27 | Spleen |
| | 14 | Muscle | 162 | Kidney | 74 | Muscle | 486 | Lung | 838 | Lung | 317 | Spleen |
| | 16 | Lung | 184 | Brain | 631 | Kidney | 788 | Lung | 192 | Muscle | 211 | Spleen |
| | 340 | Muscle | 212 | Kidney | 837 | Muscle | 563 | Liver | 50 | Muscle | 657 | Liver |
| | 341 | Muscle | 970 | Kidney | | | | | | | 718 | Spleen |
| | 572 | Muscle | 653 | Kidney | | | | | | | 743 | Spleen |
| | 94 | Muscle | 26 | Kidney | | | | | | | 969 | Spleen |
| | 97 | Muscle | 318 | Brain | | | | | | | 652 | Spleen |
| | 968 | Muscle | | | | | | | | | | |
| Correct identification rate | 9/10 | | 3/9 | | 2/5 | | 1/5 | | 2/5 | | 9/10 | |
| Incorrect identification rate | 1/10 | | 6/9 | | 3/5 | | 4/5 | | 3/5 | | 1/10 | |

^a Tissue number.

^b NNA prediction.

06EW07040. The authors would also like to thank Dr. David L. Monts for critical reading of this manuscript.

References

- [1] D.A. Cremers, L.J. Radziemski, Handbook of Laser-Induced Breakdown Spectroscopy, John Wiley & Sons, New York, 2006.
- [2] J.P. Singh, S.N. Thakur, Laser Induced Breakdown Spectroscopy, Elsevier Science B.V, Amsterdam, The Netherlands, 2007.
- [3] A. Miziolek, V. Pelleschi, I. Schechter, Laser Induced Breakdown Spectroscopy (LIBS): Fundamentals and Applications, Cambridge University Press, 2006.
- [4] M.Z. Martin, S.D. Wullschleger, C.T. Garten Jr., A.V. Palumbo, Laser-induced breakdown spectroscopy for the environmental determination of total carbon and nitrogen in soils, Appl. Opt. 42 (2003) 2072–2077.
- [5] R. Noll, H. Bette, A. Brysch, M. Kraushaar, I. Mönch, L. Peter, L. Sturm, Laser-induced breakdown spectrometry – applications for production control and quality assurance in steel industry, Spectrochim. Acta Part B 56 (2001) 637–649.
- [6] P.H. Souza, E. Munini, M.L. Redigolo, L.P. Alves, M.T.T. Pacheco, M.L. Redigolo, L.P. ALVES, M.T.T. Pacheco, Laser-induced breakdown spectroscopy in a biological tissue, Proceedings of the XXVI National Meeting of Condensed Matter Physics, Chippenham, 2003.
- [7] M.D. Adamson, S.J. Rehse, Detection of trace Al in model biological tissue with laser-induced breakdown spectroscopy, Appl. Opt. 46 (2007) 5844–5852.
- [8] V.K. Singh, V. Singh, A.K. Rai, S.N. Thakur, P.K. Rai, J.P. Singh, Quantitative analysis of gallstones using laser-induced breakdown spectroscopy, Appl. Opt. 47 (2008) G38–G47.
- [9] J.D. Hybl, G.A. Lithgow, S.G. Buckley, Laser-induced breakdown spectroscopy detection and classification of biological aerosols, Appl. Spectrosc. 57 (2003) 1207–1215.
- [10] T. Kim, Z.G. Specht, P.S. Vary, C.T. Lin, Spectral fingerprints of bacterial strains by laser-induced breakdown spectroscopy, J. Phys. Chem. B 108 (2004) 5477–5482.
- [11] S. Morel, N. Leone, P. Adam, J. Amouroux, Detection of bacteria by time resolved laser-induced breakdown spectroscopy, Appl. Opt. 42 (2003) 6184–6191.
- [12] C.A. Munson, J.L. Gottfried, E.G. Snyder, F.C. De Lucia Jr., B. Gullett, A.W. Miziolek, Detection of indoor biological hazards using the man-portable laser induced breakdown spectrometer, Appl. Opt. 47 (2008) G48–G57.
- [13] A. Kumar, F.Y. Yueh, J.P. Singh, Characterization of malignant tissue cells using laser induced breakdown spectroscopy, Appl. Opt. 43 (2004) 5399–5403.
- [14] A. Kumar, F.Y. Yueh, S. C. Burgess, J.P. Singh, Laser-induced breakdown spectroscopy for specimen analysis, US Patent Issued on August 15, 2006, US Patent No. 7092087.
- [15] J.M. Anzano, I.B. Gornushkin, B.W. Smith, J.D. Winefordner, Laser-induced plasma spectroscopy for plastic identification, Polym. Eng. Sci. 40 (2000) 2423–2429.
- [16] R. Sattmann, I. Moè Nch, H. Krause, R. Noll, S. Couris, A. Hatziaopoulou, A. Mavromanolakis, C. Fotakis, E. Larrauri, R. Miguel, Laser-induced breakdown spectroscopy for polymer identification, Appl. Spectrosc. 52 (1998) 456–461.
- [17] C. Bohling, D. Scheel, K. Hohmann, W. Schade, M. Reuter, G. Holl, Fiber-optic laser sensor for mine detection and verification, Appl. Opt. 45 (2006) 3817–3825.
- [18] J.-B. Sirven, B. Bousquet, L. Canioni, L. Sarger, S. Tellier, M. Potin-Gautier, I. Le Hecho, Qualitative and quantitative investigation of chromium-polluted soils by laser-induced breakdown spectroscopy combined with neural networks analysis, Analytical and Bioanalytical Chemistry 385 (2006) 256–262.
- [19] J. Diedrich, S.J. Rehse, S. Palchaudhuri, Escherichia coli identification and strain discrimination using nanosecond laser-induced breakdown spectroscopy, Appl. Phys. Lett. 90 (2007) 163901–163903.
- [20] J. Amador-Hernández, J.M. Fernández-Romero, M.D. Luque de Castro, In-depth characterization of screen-printed electrodes by laser-induced breakdown spectroscopy and pattern recognition, Surf. Interface Anal. 31 (2001) 313–320.
- [21] A.C. Samuels, F.C. De Lucia Jr., K.L. McNesby, A.W. Miziolek, Laser-induced breakdown spectroscopy of bacterial spores, molds, pollens, and protein: initial studies of discrimination potential, Appl. Opt. 42 (2003) 6205–6209.
- [22] M.Z. Martina, N. Labbé, T.G. Rials, S.D. Wullschleger, Analysis of preservative-treated wood by multivariate analysis of laser-induced breakdown spectroscopy spectra, Spectrochim. Acta Part B 60 (2005) 1179–1185.
- [23] J.-B. Sirven, B. Sallé, P. Mauchiena, J.-L. Lacoura, S. Maurice, G. Manhès, Feasibility study of rock identification at the surface of Mars by remote laser-induced breakdown spectroscopy and three chemometric methods, J. Anal. At. Spectrom. 22 (2007) 1471–1480.

- [24] B. Everitt, S. Landau, M. Leese, Cluster Analysis, 4th Edition, Edward Arnold Publisher, London, 2001.
- [25] M.B. Eisen, P.T. Spellman, P.O. Brown, D. Botstein, Cluster analysis and display of genome-wide expression patterns, Proc. Natl. Acad. Sci. USA 95 (1998) 14863–14868.
- [26] M.S. Aldenderfer, R.K. Blashfield, Cluster Analysis (Quantitative Applications in the Social Sciences), Sage Publications, Inc., 1984.
- [27] J.B. Plotkin, J. Chave, P.S. Ashton, Cluster analysis of spatial patterns in Malaysian tree species, The American Naturalist 160 (2002) 629–644.
- [28] R. Goodacre, É.M. Timmins, R. Burton, N. Kaderbhai, A.M. Woodward, D.B. Kell, P.J. Rooney, Rapid identification of urinary tract infection bacteria using hyperspectral, whole organism fingerprinting and artificial neural networks, Microbiology 144 (1998) 1157–1170.
- [29] É.M. Timmins, S.A. Howell, B.K. Alsberg, W.C. Noble, R. Goodacre, Rapid differentiation of closely related *Candida* species and strains by pyrolysis mass spectrometry and Fourier transform infrared spectroscopy, J. Clin. Microbiol. 36 (1998) 367–374.
- [30] OC – A Cluster Analysis Program, http://www.compbio.dundee.ac.uk/manuals/oc/oc_manual.txt.
- [31] K.H. Esbensen, Multivariate Data Analysis in Practice, 5th edition, Camo Inc, 2004.
- [32] M.I. Duran, P.A. Munoz de la, C.M.I. Rodriguez, L.F. Salinas, Simultaneous fluorometric determination of nalidixic acid and 7-hydroxymethylnalidixic acid by partial least squares calibration, Talanta 45 (1998) 899–907.
- [33] C. Chatfield, A.J. Collins, Introduction to Multivariate Analysis, Chapman & Hall, London, 1980.
- [34] J. Lawrence, Introduction to Neural Networks, 5th edition, California Scientific, Nevada City, 1993.
- [35] S. Haykin, Neural Networks: A Comprehensive Foundation, Macmillan Publishing, New York, 1994.
- [36] F. Ham, I. Kostanic, Principles of Neurocomputing for Science and Engineering, McGraw-Hill Higher Education, New York, 2001.